AIAA 81-1274R

Transient Vaporization from a Surface into Vacuum

Charles J. Knight*
Avco Everett Research Laboratory, Inc., Everett, Mass.

This paper is motivated by a general interest in pulsed energy addition to a surface in vacuum at high power fluxes ($\gtrsim 1$ MW/cm^2 absorbed). The theoretical treatment assumes a perfect gas without plasma formation, and examples are for aluminum. Transient heat conduction into the surface, vapor flux through a Knudsen layer at the surface, and transient one-dimensional flow of vapor into the surrounding vacuum are included as part of the modeling. Results show that the Knudsen layer remains choked so long as the absorbed power is constant or increasing, and it is unchoked when the absorbed power is decreasing. The problem is fully coupled in the latter case. Quasisteady vapor efflux from the surface is established within a fraction of the pulse time at sufficiently high power fluxes. Impulse coupling coefficients due to vapor recoil are noted.

I. Introduction

IT is possible to direct energy into a surface at high power density (e.g., $\gtrsim 1$ MW/cm^2) and thereby induce rapid surface vaporization. High power lasers represent one such energy source. There have been several studies of the ensuing processes when there is a surrounding air environment.[1-3] The case of a surface initially surrounded by a hard vacuum is less well studied[4,5] and is the object of this paper. The external energy source is taken to be pulsed and energy is absorbed only at the surface, or phase interface with the vapor flow region. Absorption in the vapor phase is not going to be considered even though it can be important in processes such as laser-induced breakdown.[6,7] That represents a more difficult undertaking which perhaps will be pursued in later work.

The basic methodology to be outlined is fairly general, but it is convenient to choose a particular material in order to render the discussion more concrete. An aluminum surface will be considered herein. The primary mechanisms for removing the absorbed power from the surface are typically heat conduction into the dense phase behind the surface and efflux of vapor from the surface, carrying with it the heat of vaporization. Theoretical modeling of these two processes will be discussed in turn. Then the discussion will proceed to coupling them with the transient vapor flow away from the surface.

II. Theoretical Model

At the absorbed power fluxes of interest ($\gtrsim 1$ MW/cm^2), the aluminum surface will very quickly heat up to a temperature well above the melting point. Thus, both solid and liquid phases generally will be involved in the real process, with a moving phase interface between them. This has been avoided in the analysis done here by imagining that there is only a single dense phase, a liquid. The heat of fusion for aluminum is small compared to the heat of vaporization, so the error in this idealization is not large. It has also been supposed that the thermal properties are constant. This decidedly is not true[8,9] as seen from Fig. 1. However, the approximations just noted represent considerable simplification and it can be expected that the general trends will be representative. Heat transfer into the dense phase is modeled by the linear heat conduction equation

$$\rho_l c_l \frac{\partial T}{\partial t} = k_l \frac{\partial^2 T}{\partial x^2} \tag{1}$$

where ρ_l is the liquid density, c_l its specific heat, and k_l its thermal conductivity. The possibility of convection in the liquid (driven by vapor recoil, surface tension, etc.[10]) will be overlooked.

The surface is going to recede as the aluminum boils off. This is depicted in the x-t diagram in Fig. 2, where the dense phase zone lies to the left and vapor flows in the positive x direction. It is convenient to employ a moving reference frame attached to the surface as this simplifies imposing the liquid/vapor phase jump conditions. To this end introduce $\eta = -[x + x_s(t)]$, with $x = -x_s(t)$ at the surface. The heat conduction equation becomes

$$\frac{\partial T}{\partial t} = \dot{x}_s \frac{\partial T}{\partial \eta} + \alpha_l \frac{\partial^2 T}{\partial \eta^2} \tag{2}$$

where $\alpha_l = k_l/\rho_l c_l$ is the thermal diffusivity and $\dot{x}_s = dx_s/dt$. Initially $T = T_i$ for all $\eta > 0$ and also this provides the appropriate boundary data as $\eta \to \infty$ for all $t > 0$.

Rapid surface vaporization can be modeled by means of Knudsen layer jump conditions.[11] These lead to the following

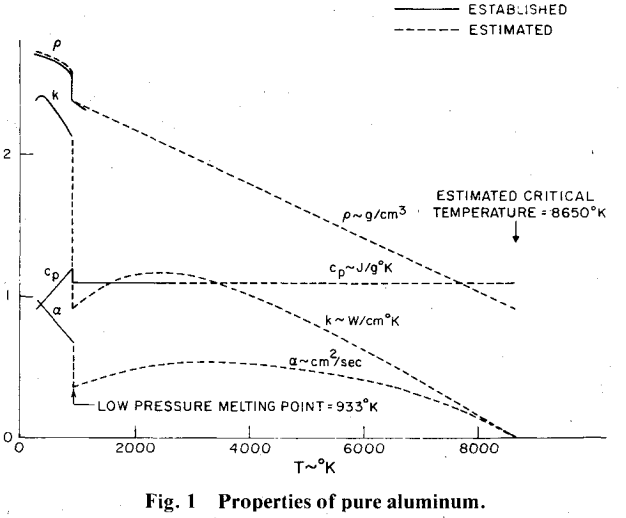

Fig. 1 Properties of pure aluminum.

Presented as Paper 81-1274 at the AIAA 14th Fluid and Plasma Dynamics Conference, Palo Alto, Calif., June 23-25, 1981; submitted July 20, 1981; revision received Nov. 16, 1981.

*Principal Research Scientist. Member AIAA.

relationships between liquid surface properties (denoted by subscript s) and vapor properties at the outer edge of the Knudsen layer where translational equilibrium is restored:

$$\frac{T}{T_s}=\left[\sqrt{1+\pi\left(\frac{\gamma-1}{\gamma+1}\frac{m}{2}\right)^2}-\sqrt{\pi}\frac{\gamma+1}{\gamma-1}\frac{m}{2}\right]^2$$

$$\frac{\rho}{\rho_s}=\sqrt{\frac{T_s}{T}}\left[\left(m^2+\frac{1}{2}\right)e^{m^2}\operatorname{erfc}(m)-\frac{m}{\sqrt{\pi}}\right]+\tfrac{1}{2}\frac{T_s}{T}\left[1-\sqrt{\pi}me^{m^2}\operatorname{erfc}(m)\right]$$

$$\rho u/\rho_s\sqrt{\frac{RT_s}{2\pi}}=1-\left(2m^2+1-m\sqrt{\frac{\pi T_s}{T}}\right)\times\left[1-\sqrt{\pi}me^{m^2}\operatorname{erfc}(m)\right] \tag{3}$$

where γ is the ratio of specific heats, $m=u/\sqrt{2RT}=M\sqrt{\gamma/2}$, and M is the flow Mach number at the outer edge of the Knudsen layer at the surface. Thermodynamic equilibrium in the liquid will be assumed so that p_s is plausibly interpreted as the saturated vapor pressure corresponding to temperature T_s. Also, $\rho_s=p_s/RT_s$ since the vapor will be treated as a perfect gas. Evaluations of Eq. (3) as a function of M are given in Table 1.

A Clausius-Clayperon relation will be adopted to relate saturated vapor pressure and temperature

$$p_s=p_b\exp\left[\frac{L_v}{RT_b}\left(1-\frac{T_b}{T_s}\right)\right] \tag{4}$$

where $p_b=1$ atm, T_b is the normal boiling temperature, and L_v is the (constant) heat of vaporization. For aluminum, $\gamma=5/3$, $T_b=2730$ K, and $L_v=11$ kJ/g are reasonable choices. The Knudsen layer model embodied in Eq. (3) leads to a vapor stagnation temperature that is always less than T_s, implying an energy flux into the liquid. However, the temperature jump is small ($\lesssim 10\%$) and will be overlooked. Thus, energy balance at the surface is taken to be expressed by

$$\left(-k_l\frac{\partial T}{\partial\eta}\right)_0+\rho uL_v=\dot{q}_a \tag{5}$$

The absorbed power per unit surface area $\dot{q}_a$ is divided between heat conduction into the liquid and latent heat carried away by the vapor. To close the problem, mass conservation requires

$$\rho_l\dot{x}_s=\rho u \tag{6}$$

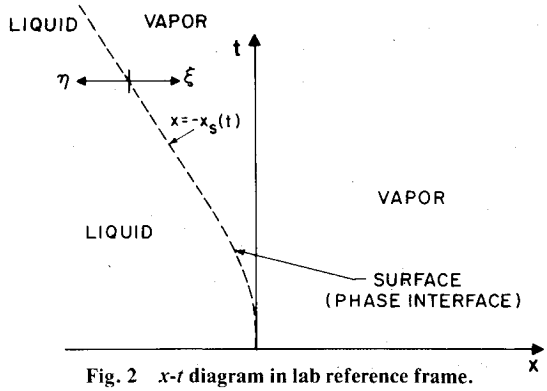

Fig. 2 x-t diagram in lab reference frame.

Table 1 Flow property ratios across Knudsen layer ($\gamma=5/3$)

M	ρ/ρ_s	T/T_s	p/p_s	$\rho u/\rho_s\sqrt{\frac{RT_s}{2\pi}}$
0	1	1	1	0
0.05	0.927	0.980	0.908	0.148
0.1	0.861	0.960	0.827	0.273
0.2	0.748	0.922	0.690	0.465
0.4	0.576	0.851	0.490	0.688
0.6	0.457	0.785	0.358	0.786
0.8	0.371	0.725	0.269	0.817
1.0	0.308	0.669	0.206	0.816

Results are best presented in terms of nondimensional variables. To this end, let τ_p be the duration of the pulse giving rise to $\dot{q}_a$ and define $\tilde{t}=t/\tau_p$, $\tilde{\eta}=\eta/\sqrt{\alpha_l\tau_p}$, $\tilde{x}_s=\dot{x}_s\sqrt{\tau_p/\alpha_l}$, $\tilde{T}=T/T_r$, $\tilde{u}=u/a_r$, $\tilde{p}=p/p_r$, and $\tilde{\rho}=\rho/\rho_r$. Natural choices for the reference parameters are $T_r=T_b\sim 2730$ K, $a_r=\sqrt{\gamma RT_b}\sim 1.2\times10^5$ cm/s, $p_r=p_b=1$ atm, and $\rho_r=p_b/RT_b\sim 1.2\times10^{-4}$ g/cm^3. This leads to six basic nondimensional parameters: T_i/T_b, γ, L_v/RT_b, L_v/c_lT_b, $\dot{Q}\sqrt{\alpha_l\tau_p}/k_lT_b$, and $\rho_ra_r/\rho_l\sqrt{\tau_p/\alpha_l}$ where $\dot{Q}$ is a characteristic absorbed power flux. Only the case of a top-hat absorbed power flux is considered in this paper

$$\dot{q}_a=\dot{Q}, \qquad 0<t<\tau_p$$
$$=0, \qquad t>\tau_p \tag{7}$$

Representative values of the thermal properties for liquid aluminum are $\rho_l\sim 1.6$ g/cm^3, $c_l\sim 1.1$ J/g K, $k_l\sim 0.80$ W/cm K, and $\alpha_l\sim 0.45$ cm^2/s. Also, $T_i\sim 300$ K is an interesting initial condition. These were used in evaluating the nondimensional parameters for what follows.

In general the problem just defined is coupled to the exterior vapor flow through the Mach number at the outer edge of the Knudsen layer M. However, the processes are decoupled so long as the Knudsen layer remains choked (i.e., $M=1$). This special case will be examined before going on to the fully coupled case. As will be seen later, the Knudsen layer remains choked only during a top-hat pulse and not afterwards. Results for this special case were generated numerically for $\tau_p=1$ μs and are shown in Fig. 3. It was necessary to use an implicit differencing procedure for an economical treatment. Note that the surface temperature approaches an asymptote during the pulse for $\dot{Q}>10$ MW/cm^2. That steady state is defined by a balance between

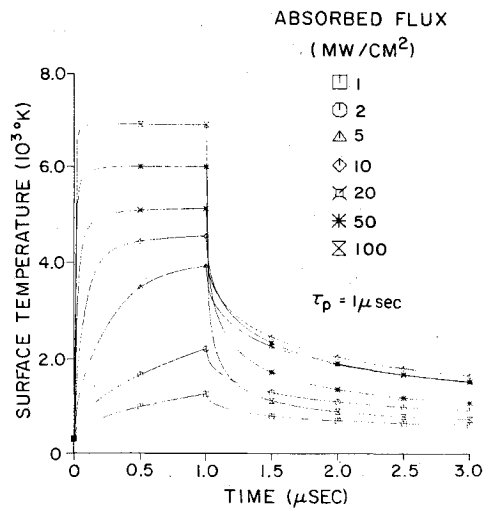

Fig. 3 Conduction solutions for a choked Knudsen layer and various top-hat absorbed fluxes.

the advection and diffusion terms on the right side of Eq. (2). Note also that this steady state is reached increasingly rapidly as $\dot{Q}$ increases. The heat up (or cool down) time scales inversely as $\dot{Q}^2$, as might be expected from the fact that $\dot{Q}\sqrt{\tau_p}$ enters one of the nondimensional parameters given earlier.

A straightforward analysis leads to the following steady-state distribution of temperature in the liquid.

$$T = T_i + (T_s - T_i)\exp(-\dot{x}_s \eta/\alpha_l) \tag{8}$$

Mass and energy balance at the surface then leads to

$$[c_l(T_s - T_i) + L_v]\frac{\phi p_s}{\sqrt{2\pi R T_s}} = \dot{Q} \tag{9}$$

for a time invariant absorbed power $\dot{Q}$, where $\phi = 0.816$ is the normalized mass flux for choked conditions (cf. Table 1). This nonlinear algebraic equation has been solved numerically to generate the results in Table 2. Note that the saturated vapor pressure at steady state increases essentially linearly with $\dot{Q}$ whereas T_s increases logarithmically in accordance with Eq. (4). The predicted steady-state surface temperature is well above critical conditions (cf. Fig. 1) for $\dot{Q} = 1$ GW/cm^2, and the prediction is then highly questionable for a variety of reasons. The model predictions are viewed as meaningful for aluminum only when the absorbed power flux $\dot{q}_a \lesssim 100$ MW/cm^2.

Turn now to the modeling for the vapor flow outside the Knudsen layer. The vapor will be treated as a nonabsorbing perfect gas, as mentioned earlier. It is again convenient to employ a moving reference frame attached to the surface. In terms of $\xi = x + x_s(t)$, the equations of motion become

$$\frac{\partial \rho}{\partial t} + \frac{\partial}{\partial \xi}(\rho u) = 0$$

$$\rho\left(\frac{\partial u}{\partial t} + u\frac{\partial u}{\partial \xi}\right) + \frac{\partial p}{\partial \xi} = \rho \ddot{x}_s$$

$$\rho c_v\left(\frac{\partial T}{\partial t} + u\frac{\partial T}{\partial \xi}\right) + p\frac{\partial u}{\partial \xi} = 0 \tag{10}$$

In the case of the top-hat energy input in Eq. (7) and a surrounding hard vacuum, no shocks will appear anywhere within the flowfield. A method of characteristics then provides the best approach to solving for the exterior flow. Characteristic equations following from Eq. (10) are

$$\frac{dP}{dt} = \frac{a}{\gamma R}\frac{ds}{dt} + \ddot{x}_s \quad \text{on} \quad \frac{d\xi}{dt} = u + a$$

$$\frac{dQ}{dt} = \frac{a}{\gamma R}\frac{ds}{dt} - \ddot{x}_s \quad \text{on} \quad \frac{d\xi}{dt} = u - a$$

$$\frac{ds}{dt} = 0 \quad \text{on} \quad \frac{d\xi}{dt} = u \tag{11}$$

where $P = 2a/(\gamma - 1) + u$ and $Q = 2a/(\gamma - 1) - u$ are the Riemann invariants and s the entropy. The directions in the first two of these equations will be referred to as P and Q characteristics, respectively.

So long as the Knudsen layer remains choked (i.e., $M = 1$), determination of surface conditions is independent of the exterior vapor flow. In that case the external flow follows by a straightforward marching procedure into $\xi > 0$, starting with known conditions at the outer edge of the Knudsen layer at $\xi = 0$. (The Knudsen layer is viewed as having infinitesimal thickness in this paper.) Note that Q characteristics start with zero slope at $\xi = 0$ and that the slope will gradually become positive in $\xi > 0$. The solution domain always lies to the left of the terminal P characteristic on which $a = 0$ and u assumes an extremal value. The situation just outlined is found to persist so long as the absorbed power flux is monotonically increasing or constant in time.

Table 2 Steady state results for $M = 1$

$\dot{Q}$, MW/cm^2	T_s, K	p_s, atm
0.1	2,890	2.07
1	3,570	21.8
10	4,670	230
100	6,750	2,420
1,000	11,980	24,400

If the Knudsen layer is not choked, as will happen when $\dot{q}_a$ decreases, one or more of the characteristics will have a negative slope. This involves only the Q characteristic for $0 < M < 1$. That is the only situation considered in this paper even though condensation ($M < 0$) can arise, as will be seen later. When $0 < M < 1$, the compatibility relation along a Q characteristic provides information determining M and hence the surface state.[11] Heat conduction, surface balance relations, and the exterior vapor flow are thereby coupled. Once the surface state is established, the rest of the exterior flow is obtained by the same sort of marching procedure noted in the preceding paragraph.

III. Results and Discussion

A typical evolution of surface properties is displayed in Fig. 4 for $\tau_p = 1$ μs and $\dot{Q} = 10$ MW/cm^2. Note that the Mach number at the outer edge of the Knudsen layer drops rapidly to zero shortly after the pulse. The possibility of $u < 0$ at the surface is disallowed because condensation has not been included in the modeling. Here $u = 0$ is imposed artificially for $\tilde{t} > 1.2$, so the results for large values of $\tilde{t}$ are suspect. The surface temperature after the pulse is significantly different from that in Fig. 3, where $M = 1$ at all times is (incorrectly) assumed.

The saturated vapor pressure is also shown in Fig. 4. This does not define directly the force acting on the surface. Neglecting the momentum of the liquid, $\rho_l(\dot{x}_s)^2$, this is given by the momentum flux of vapor from the Knudsen layer: $F = p + \rho u^2 = p(1 + \gamma M^2)$. The value of F is roughly 55% of p_s for a choked Knudsen layer and can be evaluated using Table 1 more generally. Also shown in Fig. 4 is the normalized mechanical impulse delivered to the surface,

$$\int_0^{\tilde{t}} \tilde{F} d\tilde{t}$$

with $\tilde{F} = F/p_b$. Essentially all the impulse, when the surface is surrounded by vacuum, appears to be delivered during the pulse. This result conceivably could be altered if condensation is properly modeled, but plasma effects are expected to be considerably more important.

Flow properties in the exterior flow at the end of the pulse ($\tilde{t} = 1$) are given in Fig. 5 for $\tau_p = 1$ μs and $\dot{Q} = 10$ MW/cm^2. Such information provides a quantitative basis for assessing whether plasma formation, due to processes such as laser-induced breakdown, is likely. When the surface is surrounded by ambient air, plasma effects can increase or decrease the impulse coupling, depending on the conditions involved.[1] The corresponding situation with a surrounding vacuum needs more experimental and theoretical study.

The rapidity of pressure decrease after the pulse seen in Fig. 4 makes one wonder about blowoff of a portion of the liquid layer due to internal vapor bubble formation. The dense

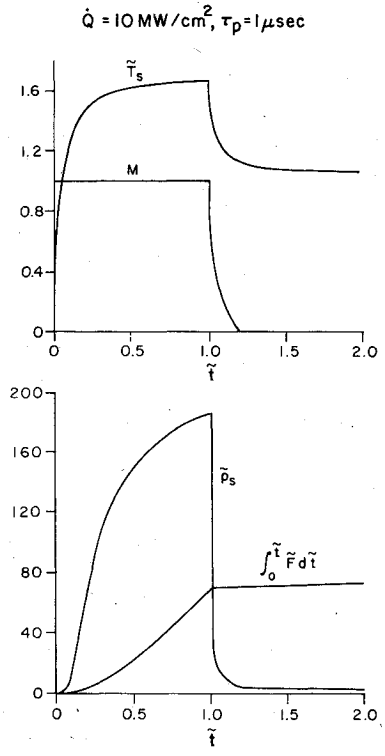

Fig. 4 Evolution of surface properties for coupled conduction and vapor flow modeling.

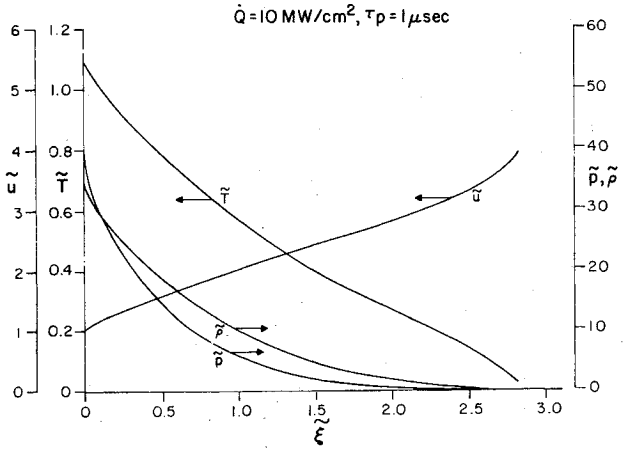

Fig. 5 Properties in exterior flow at the end of a 1 μs pulse.

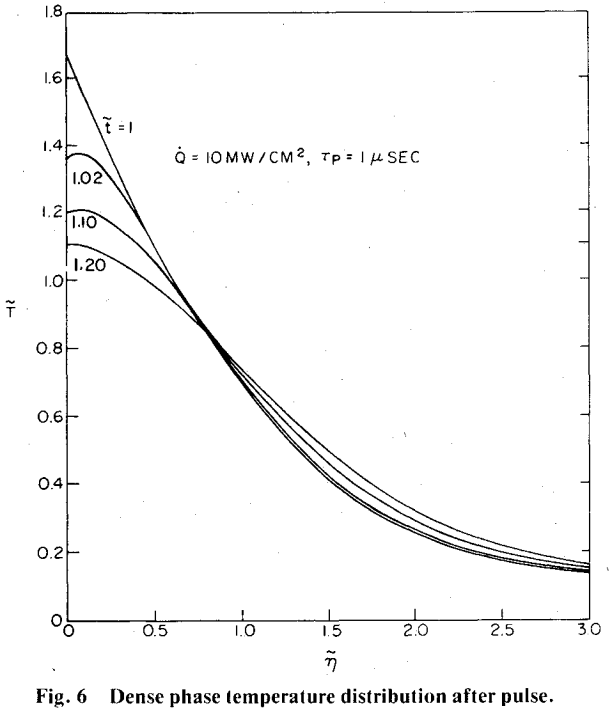

Fig. 6 Dense phase temperature distribution after pulse.

phase temperature profiles given in Fig. 6 provide a basis for assessing this. The possibility of bubble formation arises because there is a maximum temperature in $\eta > 0$ and hence a zone in which the vapor pressure is higher than that at the phase interface. The liquid cannot support a negative pressure differential in general. However, the small pressure differentials involved ($\lesssim 2$ atm) and the short duration of the negative differential make ejection of a layer of liquid doubtful. Melt splash is observed experimentally, in the form of a rim crater around a finite laser spot, but this is believed to be due to transverse liquid flow induced by the large overpressure during the pulse.[5] This and other two- and three-dimensional effects can be overlooked for sufficiently large spot sizes.

The baseline mean thermal properties noted in Sec. II were used in generating these results: $\rho_l = 1.6$ g/cm^3, $c_l = 1.1$ J/g K, $k_l = 0.80$ W/cm K, and $\alpha_l = 0.45$ cm^2/s. In view of Fig. 1, the effect of varying these properties should be examined. It turns out that only two of the nondimensional groups involved in the problem are particularly sensitive: $\dot{Q}\sqrt{\alpha_l \tau_p}/k_l T_b$ and $\rho_r a_r / \rho_l \sqrt{\tau_p/\alpha_l}$. Also, they are roughly proportional to each other since the specific heat for aluminum varies little with temperature. Thus, the sensitivity analysis is done adequately by varying a single parameter, $\sqrt{\alpha}/k$. Calculated values of the mechanical impulse delivered during a top-hat absorbed energy input are given in Table 3 for the conditions of Fig. 4. There is an order-of-magnitude variation in impulse depending on whether solid-state properties are used ($\alpha \sim 0.84$ cm^2/s, $k \sim 2.3$ W/cm K) or liquid properties at 7000 K are used ($\alpha \sim 0.3$ cm^2/s, $k \sim 0.4$ W/cm K). This provides impetus to account for temperature-dependent dense phase properties in later work. That will require adding at least a continuity equation for the dense phase if the advection term is to be calculated properly. Results presented hereafter involve the baseline mean properties.

Table 3 Impulse sensitivity to dense phase properties for absorbed flux = 10 MW/cm^2 and $\tau_p = 1$ μs

$\frac{0.8}{k_l}\sqrt{\frac{\alpha_l}{0.45}}$	0.45	0.75	1	1.30	1.65
$\int_0^{\tilde{t}} \tilde{F} d\tilde{t}$	10.9	47.9	69.4	85.9	93.1

The impulse coupling coefficient C is one parameter relevant to understanding damage mechanisms associated with pulsed devices interacting with a surface. This is defined normally in terms of the incident power flux, $\dot{q}_i$, but here it will be given in terms of $\dot{q}_a$ which is typically a fraction of $\dot{q}_i$. A subscript a will be appended to emphasize this unconventional definition. Thus,

$$C_a = \int_0^{t_{\max}} \frac{F dt}{\dot{Q}\tau_p} \tag{12}$$

for a top-hat input. Usually, $t_{\max} = \infty$ is used to account for impulse accrued after the pulse. Here $t_{\max} = \tau_p$ is used, which is believed to involve little error in view of Fig. 4. The predicted coupling coefficient due to vapor recoil is given in Fig. 7 for three pulse durations. Note that C_a is relatively insensitive to $\dot{Q}$ at the larger absorbed power fluxes. The

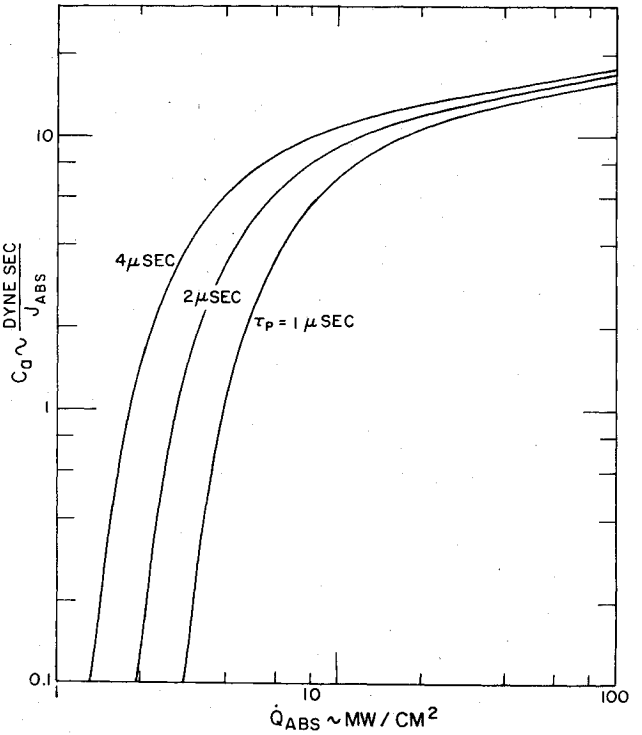

Fig. 7 Impulse coupling coefficient due to vapor recoil.

reason is simple; steady-state conditions prevail essentially throughout the pulse, as expected from Fig. 3. This decidedly is not true for smaller values of $\dot{Q}$.

The thermal coupling coefficient is important in situations involving more than one pulse. This normally is defined as the ratio of energy remaining in the surface long after a single pulse divided by the incident energy. It is important because the surface temperature can build up in a repetitively pulsed situation. Here again an unconventional definition is adopted in dividing by the absorbed rather than incident energy. For a top-hat input,

$$C_{T_a} = \int_0^\infty \rho_l c_l (T_s - T_i)\, d\eta / \dot{Q}\tau_p \qquad (13)$$

Predicted values of the thermal coupling coefficient are given in Table 4 for $\tau_p = 1$ μs. Note that most of the absorbed power is carried away by the vapor at the higher flux densities.

IV. Conclusion

A theoretical model has been constructed including two of the primary mechanisms influencing pulsed vaporization of an aluminum surface into a surrounding vacuum. There are elements that need improvement; for example, variable thermal properties of the dense phase, real gas effects near the critical point, and treatment of condensation. The important point, however, is that it provides the infrastructure needed to model quantitatively another possible process: plasma formation, including absorption and radiative energy transfer in the vapor. This may be pursued in future work. A summary of the conclusions reached in this paper follows.

1) Heat conduction and vapor efflux generally represent equally important mechanisms for removing absorbed power from the surface or liquid/vapor interface.

2) The surface heat-up time varies inversely with the square of the absorbed power flux and easily can be small compared to the pulse duration.

3) The Knudsen layer, attached to the surface, tends to be choked when the absorbed power is constant or increasing and unchoked when the power is decreasing. The problem is fully coupled when the Knudsen layer is unchoked.

Table 4 Thermal coupling coefficient for $\tau_p = 1$ μs

$\dot{Q}$, MW/cm^2	3	10	30	100
$\frac{k_l T_b}{\dot{Q}\sqrt{\alpha_l \tau_p}} \int_0^\infty (\tilde{T}_s - \tilde{T}_i)\, d\tilde{\eta}$	1.00	0.467	0.126	0.021

Acknowledgments

The author wishes to express his thanks to A. Ballantyne and J. Woodroffe for many useful discussions during the course of this study. A. Ballantyne assembled the data on which Fig. 1 is based. This work was supported by the Defense Advanced Research Projects and was monitored by the U. S. Army Missile Command under Contract DAAH01-80-C-1523.

References

[1] Reilly, J., Ballantyne, A., and Woodroffe, J., "Modeling of Momentum Transfer to a Surface by Laser Supported Absorption Waves," *AIAA Journal*, Vol. 17, Oct. 1979, pp. 1098-1105.

[2] Pirri, A. N., Root, R. C., and Wu, P. K. S., "Plasma Energy Transfer to Metal Surfaces Irradiated by Pulsed Lasers," *AIAA Journal*, Vol. 16, Dec. 1978, pp. 1296-1304.

[3] Woodroffe, J., Hsia, J., and Ballantyne, A., "Thermal and Impulse Coupling to an Aluminum Surface by a Pulsed KrF Laser," *Applied Physics Letters*, Vol. 36, No. 1, 1980, pp. 14-15.

[4] Rosen, D., Mittledorf, J., Kothandaraman, G., Pirri, A., and Pugh, E., "Coupling of Pulsed 0.35 μm Laser Radiation with Aluminum Alloys," AIAA Paper 80-1321, July 1980.

[5] Duzy, C., Woodroffe, J. A., Hsia, J., and Ballantyne, A., "Interaction of a Pulsed XeF Laser with an Aluminum Surface," *Applied Physics Letters*, Vol. 37, No. 6, 1980, pp. 542-544.

[6] Shui, V., Kivel, B., and Weyl, G., "Effect of Vapor Plasma on the Coupling of Laser Radiation with Aluminum Targets," *Journal of Quantum Spectroscopy and Radiative Transfer*, Vol. 20, No. 6, 1978, pp. 627-636.

[7] Weyl, G., Pirri, A., and Root, R., "Laser Ignition of Plasma off Aluminum Surfaces," AIAA Paper 80-1319, July 1980.

[8] Touloukian, Y., (series ed.), *Thermophysical Properties of Matter*, Purdue University, Vol. 1, IFI/Plenum, 1970.

[9] Grosse, A., "Electrical and Thermal Conductivities of Metals over Their Entire Liquid Range," *Revue des Hautes Temperatures et des Refractaires*, Vol. 3, No. 6, 1966, pp. 115-146.

[10] Palmer, H., "The Hydrodynamic Stability of Rapidly Evaporating Liquids at Reduced Pressure," *Journal of Fluid Mechanics*, Vol. 75, Part 3, 1976, pp. 487-512.

[11] Knight, C. J., "Theoretical Modeling of Rapid Surface Vaporization with Back-Pressure," *AIAA Journal*, Vol. 17, May 1979, pp. 519-523.